Analysis of current and shot noise correlations in a double quantum dot interferometer with interdot spin interactions

Marko Zivkovic, Brandon W. Langley, Ivana Djuric, and Chris P. Search*

Department of Physics and Engineering Physics, Stevens Institute of Technology, Castle Point on Hudson, Hoboken, New Jersey 07030, USA

(Received 27 August 2010; published 4 March 2011)

We examine an electron Aharonov-Bohm (AB) interferometer with individual quantum dots connected in parallel to macroscopic leads. Here, we focus on the effect that both interdot spin-spin exchange interactions and intradot spin flips have on the current- and frequency-dependent current shot noise. By appropriate control of AB magnetic flux, interdot Coulomb repulsion, intradot spin flips, and interdot spin-spin coupling, the probability amplitudes for the different paths of the interferometer can be controlled, leading to broad tunability of both the shape and the contrast of interference fringes in the current. We also show that in the shot noise at finite frequencies corresponding to the spin-spin interaction energies, the noise shows a pronounced super-Poissonian and sub-Poissonian structure. AB flux, which is not an integer multiple of 2π, dramatically suppresses the correlations in the shot noise.

DOI: 10.1103/PhysRevB.83.115304 PACS number(s): 73.63.Kv, 73.23.−b

I. INTRODUCTION

The analysis of shot noise in mesoscopic circuits[1] has became an important topic in transport since it is a direct measure of interparticle correlations and therefore indicates additional information about processes in the circuit that cannot be obtained directly from standard conductance measurements such as Coulomb interactions, quantum statistics of charge carriers, available transport channels, and entanglement. Such effects cause the shot noise to differ from the "classical" Poissonian noise for uncorrelated transport of discrete charge carriers by leading either to a bunching in the arrival times of charge carriers (super-Poissonian statistics) or to antibunching (sub-Poissonian statistics). Moreover, while the DC (zero-frequency) shot noise measures the long-time steady-state correlations in the arrival times of the charge carriers, measurement of the shot noise at nonzero frequencies provides a method for measuring correlations over finite time intervals, which reveal the time scales of dynamical processes in the circuit.

Over the last several decades, Aharonov-Bohm (AB) interferometers have become a paradigm of phase-coherent transport and quantum interference in solid-state nanostructures.[2,3] In this paper, we analyze an electron AB interferometer consisting of two quantum dots (QDs) connected in parallel to two macroscopic leads such as have been demonstrated experimentally.[4–8] The roles of quantum interference and Coulomb interactions in conductance have been studied using both quantum rate equations (also known as master equations)[9–12] and Greens function technique.[13–16] Earlier theoretical work has also studied the zero-frequency shot noise in these structures.[17–21]

What distinguishes our work from prior work is the study of spin-dependent transport with the inclusion of an interdot spin exchange interaction and, also, the evaluation of the finite-frequency shot noise. We show here that the the inclusion of spin-spin interactions, while having no effect on the current-voltage (I-V) curve or zero-frequency shot noise, do lead to significant correlations in the finite-frequency noise revealing the internal spin dynamics of the interferometer. Both super- and sub-Poissonian correlations, which occur at frequencies corresponding to the intradot spin-flip Rabi frequencies and inter-dot spin-spin coupling energies, can be further controlled by tuning the magnetic flux through the interferometer. These shot noise correlations occur when each dot is simultaneously occupied by a single electron, which leads to a vanishing of interference fringes in the conductance since intradot Coulomb blockade prevents the partitioning of a single electron's wave function between dots. However, modulation of the shot noise by the AB magnetic flux even in this doubly occupied regime indicates that the relative phase between the electrons still affects the correlation between their tunneling times out of the interferometer. Our approach is based on a master equation for the transport through the dots combined with the quantum regression theorem[23] to calculate the shot noise in the manner originally developed in Refs. 24 and 25.

The rest of the paper is organized in the following way. In Sec. II we review the model of our system and describe the method used to derive the results. In Sec. III we present and discuss the results; this section is divided into two parts—one considers only results involving zero-flux AB flux and the other the effects of a finite AB flux. Section IV summarizes our conclusions.

II. MODEL

Our model represents a ballistic electron AB interferometer with a single QD embedded in each of the two arms of the interferometer. As shown in Fig. 1 both arms are connected in parallel to leads via tunnel barriers. An adjustable bias is applied across the leads, allowing the flow of current between them by sequential tunneling of electrons through the dots. Due to the infinite intradot Coulomb blockade that we consider, only a single electron can occupy a dot, while interdot Coulomb charging is finite, allowing for double occupancy of the interferometer. An external magnetic field is applied perpendicular to the interferometer, leading to a magnetic flux Φ and Zeeman splitting within the dots. A transverse oscillating radio-frequency magnetic field in the plane of the interferometer allows for intradot Rabi oscillations between two spin levels with Rabi frequencies R_1 and R_2 for dot 1 and dot 2, respectively. Finally, we assume the presence

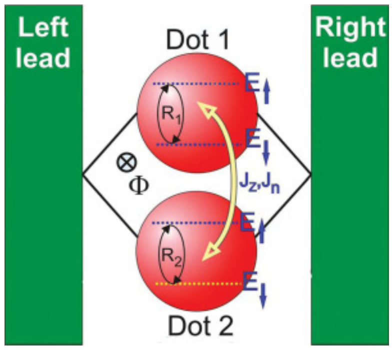

FIG. 1. (Color online) Model of our system showing two parallel quantum dots coupled to leads with spin exchange interaction between dots. A magnetic field in the region between dots provides a relative phase between electrons in the different dots as a result of the Aharonov-Bohm effect.

of a direct exchange interaction between dots, leading to a Heisenberg Hamiltonian for the spins of the two dots in the case of double occupancy characterized by two parameters: the longitudinal coupling (J_z), causing a nonlinear Zeeman shift, and a transversal coupling strength (J_n), which flips the spins. The exchange interaction could arise naturally from tunneling of electrons between dots[26] but also could be induced by, for example, coupling to a superconducting microstrip resonator[27] or by two-photon Raman transitions in an optical microcavity.[28,29]

The Hamiltonian for the two-dot system is given by[29]

$$\begin{aligned}\hat{H} &= U\hat{n}_1\hat{n}_2 + \sum_{i=1,2}(E_{D,i}\hat{n}_i + \hbar\Omega_i\hat{s}_{i,z}) + \frac{J_n}{2\hbar}(\hat{s}_1^+\hat{s}_2^- + \hat{s}_1^-\hat{s}_2^+)\\ &+ \frac{J_z}{\hbar}\hat{s}_{1,z}\hat{s}_{2,z} + R_1(e^{-i\omega_B t}\hat{s}_1^+ + e^{i\omega_B t}\hat{s}_1^-)\\ &+ R_2(e^{-i\omega_B t}\hat{s}_2^+ + e^{i\omega_B t}\hat{s}_2^-), \end{aligned} \tag{1}$$

where U is the interdot Coulomb repulsion, Ω_i is the Zeeman splitting, and $E_{D,i}$ is the orbital energy level in dot i. $R_1 = -g_1\mu_B B_n/\hbar$ and $R_2 = -g_2\mu_B B_n/\hbar$ are the Rabi frequencies for dot 1 and dot 2, respectively, of the transverse magnetic field oscillating at frequency ω_B. The operator $\hat{n}_i$ represents the occupation number of dot i, while $\hat{s}_{i,z} = \hat{c}^\dagger_{i,\uparrow}\hat{c}_{i,\uparrow} - \hat{c}^\dagger_{i,\downarrow}\hat{c}_{i,\downarrow}$ $\hat{s}_i^- = \hat{c}^\dagger_{i,\downarrow}\hat{c}_{i,\uparrow}$, $\hat{s}_i^+ = \hat{c}^\dagger_{i,\uparrow}\hat{c}_{i,\downarrow}$ are the spin operators for an electron in dot i and $\hat{c}_{i,\sigma}$ is a spin-σ electron annihilation operator for dot i.

After transforming the spin operators to a frame rotating at the transverse field frequency ω_B, the Hamiltonian becomes

$$\begin{aligned}\hat{H} &= U\hat{n}_1\hat{n}_2 + \sum_{i=1,2}(\bar{E}_D\hat{n}_i + \Delta\hat{s}_{i,z}) + \frac{J_n}{2\hbar}(\hat{s}_1^+\hat{s}_2^- + \hat{s}_1^-\hat{s}_2^+)\\ &+ \frac{J_z}{\hbar}\hat{s}_{1,z}\hat{s}_{2,z} + R_1(\hat{s}_1^+ + \hat{s}_1^-)\\ &+ R_2(\hat{s}_2^+ + \hat{s}_2^-), \end{aligned} \tag{2}$$

where $\Delta = \bar{\Omega} - \omega_B$ is the detuning of the radio-frequency magnetic field relative to the average Zeeman splitting. We have assumed that the differences in the orbital energy levels and Zeeman splitting of the dots are small compared to all other characteristic energies, $|E_{D,1} - E_{D,2}|, |\Omega_1 - \Omega_2| \ll \bar{E}_D, \bar{\Omega}, R_1, R_2, J_n, J_z$, so that henceforth we can assume that the differences can be neglected and the average orbital and Zeeman energies, $\bar{E}_D$ and $\bar{\Omega}$, can be used instead. This approximation is important for operation of the device as an interferometer since, for large $|E_{D,1} - E_{D,2}|$, $|\Omega_1 - \Omega_2|$, the symmetry between paths of the interferometer with respect to the leads is ruined and there is no longer any observable interference.

The energy diagram of our system is presented in Fig. 2(b), along with the transition energies ΔE in Fig. 2(a), representing the energy required to add an additional electron to the device from the leads. These are the energies that an electron in a lead needs to have to tunnel into one of the two spin states of an empty dot. In the case of one empty and one occupied dot, the interdot Coulomb repulsion U between electrons increases the energy needed for an electron to enter the empty dot by U to $E_D \pm \Omega + U$. Naturally, this increases the energy levels of our system [shown in Fig. 2(b)] for doubly occupied states.

The coupling between the leads and the dots is described by the Hamiltonian[9–16,18–21]

$$\begin{aligned}\hat{H}_{\text{lead-dot}} &= \sum_{k,\sigma}(t_{L1\sigma}\hat{d}^\dagger_{Lk\sigma}\hat{c}_{1,\sigma} + t_{R1\sigma}\hat{d}^\dagger_{Rk\sigma}\hat{c}_{1,\sigma} + \text{H.c.})\\ &+ \sum_{k,\sigma}(t_{L2\sigma}\hat{d}^\dagger_{Lk\sigma}\hat{c}_{2,\sigma} + t_{R2\sigma}\hat{d}^\dagger_{Rk\sigma}\hat{c}_{2,\sigma} + \text{H.c.}), \end{aligned} \tag{3}$$

where $\hat{d}_{L(R)k\sigma}$ is the annihilation operator for an electron in the left(right) lead with momentum k and spin σ, and $t_{L(R)i\sigma}$ is the tunneling amplitude of that electron across the tunnel barrier into the ith dot. The AB phase Φ due to the magnetic flux is be incorporated into the tunneling amplitudes,[9–16] $t^*_{L1\sigma} = t_{L2\sigma} = t^*_{R2\sigma} = t_{R1\sigma} = |t|e^{i\Phi/4}$, where we assume for simplicity that the tunneling amplitudes are the same for both leads.

To incorporate the coupling of the dots to the left and right macroscopic leads, we introduce the density matrix whose elements are defined as

$$\rho_{\sigma_1',\sigma_2',\sigma_1,\sigma_2} = \langle\sigma_1',\sigma_2'|\,\hat{\rho}\,|\sigma_1,\sigma_2\rangle, \tag{4}$$

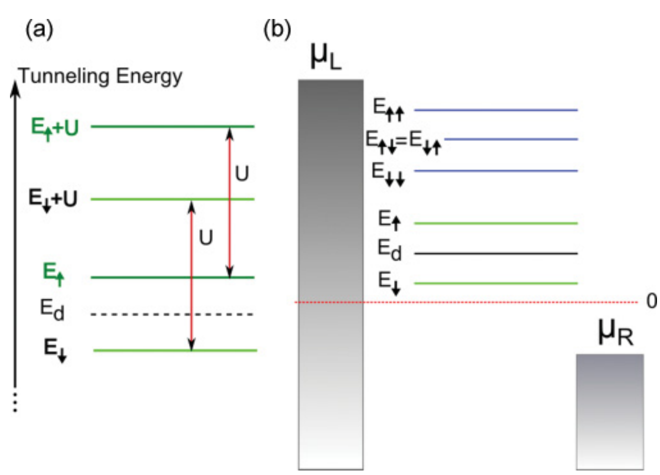

FIG. 2. (Color online) Depiction of energy parameters of interest in our model (not to scale): (a) diagram of tunneling energies; (b) energy eigenstates of the double dot for $R_1 = R_2 = J_n = J_z = 0$. E_σ represents a single spin-polarized electron in the interferometer with spin σ, while $E_{\sigma\sigma'}$ represents one electron in each of the dots with spins σ and σ'.

where $|\sigma_1,\sigma_2'\rangle$ represents a state with an electron with spin $\sigma_1 = 0, \uparrow, \downarrow$ in the first dot and an electron with spin $\sigma_2' = 0, \uparrow, \downarrow$ in the second dot (0 indicates an empty dot). The time evolution of ρ is given by a Born-Markov master equation consisting of two parts:

$$\dot{\rho} = -(i/\hbar)[\hat{H},\rho] + L[\rho]. \tag{5}$$

Here the first term of the master equation represents the unitary evolution due to the Hamiltonian. The second part represents the coupling to the leads, which can be derived from $\hat{H}_{\text{lead-dot}}$ using either Greens functions[9,22] or second-order perturbation theory on the density operator:[25]

$$\begin{aligned}
\dot{\rho}_{00,00} &= \sum_{\sigma}[-2\alpha_{1\sigma}\rho_{00,00} + \beta_{1\sigma}(\rho_{\sigma0,\sigma0} + \rho_{0\sigma,0\sigma}) \\
&\quad + \beta_{2\sigma}\rho_{\sigma0,0\sigma} + \beta_{2\sigma}^*\rho_{0\sigma,\sigma0}], \\
\dot{\rho}_{\sigma0,\sigma0} &= \alpha_{1\sigma}\rho_{00,00} - \left(\beta_{1\sigma} + \sum_{\sigma'}\tilde{\alpha}_{1\sigma'}\right)\rho_{\sigma0,\sigma0} \\
&\quad - 1/2(\beta_{2\sigma} + \tilde{\alpha}_{2\sigma})\rho_{\sigma0,0\sigma} - 1/2(\beta_{2\sigma}^* + \tilde{\alpha}_{2\sigma}^*)\rho_{0\sigma,\sigma0} \\
&\quad + \sum_{\sigma'}\tilde{\beta}_{1\sigma'}\rho_{\sigma\sigma',\sigma\sigma'}, \\
\dot{\rho}_{0\sigma,0\sigma} &= \alpha_{1\sigma}\rho_{00,00} - \left(\beta_{1\sigma} + \sum_{\sigma'}\tilde{\alpha}_{1\sigma'}\right)\rho_{0\sigma,0\sigma} \\
&\quad - 1/2(\beta_{2\sigma} + \tilde{\alpha}_{2\sigma})\rho_{\sigma0,0\sigma} - 1/2(\beta_{2\sigma}^* + \tilde{\alpha}_{2\sigma}^*)\rho_{0\sigma,\sigma0} \\
&\quad + \sum_{\sigma'}\tilde{\beta}_{1\sigma'}\rho_{\sigma'\sigma,\sigma'\sigma}, \\
\dot{\rho}_{0\sigma,\sigma0} &= \alpha_{2\sigma}\rho_{00,00} - 1/2(\beta_{2\sigma} + \tilde{\alpha}_{2\sigma})(\rho_{\sigma0,\sigma0} + \rho_{0\sigma,0\sigma}) \\
&\quad - \left(\beta_{1\sigma} + \sum_{\sigma'}\tilde{\alpha}_{1\sigma'}\right)\rho_{0\sigma,\sigma0} + \tilde{\beta}_{2\sigma}\rho_{\sigma\sigma,\sigma\sigma}, \\
\dot{\rho}_{\sigma\sigma,\sigma\sigma} &= \tilde{\alpha}_{1\sigma}(\rho_{\sigma0,\sigma0} + \rho_{0\sigma,0\sigma}) + \tilde{\alpha}_{2\sigma}\rho_{\sigma0,0\sigma} \\
&\quad + \tilde{\alpha}_{2\sigma}^*\rho_{0\sigma,\sigma0} - 2\tilde{\beta}_{1\sigma}\rho_{\sigma\sigma,\sigma\sigma}, \\
\dot{\rho}_{\sigma\bar{\sigma},\sigma\bar{\sigma}} &= \tilde{\alpha}_{1\sigma}\rho_{0\bar{\sigma},0\bar{\sigma}} + \tilde{\alpha}_{1\bar{\sigma}}\rho_{\sigma0,\sigma0} - (\tilde{\beta}_{1\sigma} + \tilde{\beta}_{1\bar{\sigma}})\rho_{\sigma\bar{\sigma},\sigma\bar{\sigma}},
\end{aligned} \tag{6}$$

where tunneling rates $\alpha_{1\sigma}(\tilde{\alpha}_{1\sigma})$ model the tunneling out of the leads into singly(doubly) occupied dot states, while $\alpha_{2\sigma}(\tilde{\alpha}_{2\sigma})$, by contrast, model the tunneling out of the leads into a superposition of singly(doubly) occupied states, respectively, where the wave function of the entering electron is split between the dots. Coefficients $\beta_{1\sigma}(\tilde{\beta}_{1\sigma})$ and $\beta_{2\sigma}(\tilde{\beta}_{2\sigma})$ are the tunneling rates out of singly(doubly) occupied dots and the appropriate superpositions into the leads. These tunneling rates are given explicitly in terms of the Fermi-Dirac distribution of the leads $f_{L(R)}(\epsilon)$, the probability per unit time of an electron crossing the tunnel barrier from the lead into one of the dots, or vice versa, $\Gamma_{L(R)\sigma} \propto |t|^2$, and the AB magnetic flux enclosed by the interferometer Φ:

$$\begin{aligned}
\alpha_{1\sigma} &= f_L(E_\sigma)\Gamma_{L\sigma} + f_R(E_\sigma)\Gamma_{R\sigma}, \\
\beta_{1\sigma} &= (1 - f_L(E_\sigma))\Gamma_{L\sigma} + (1 - f_R(E_\sigma))\Gamma_{R\sigma}, \\
\tilde{\alpha}_{1\sigma} &= f_L(E_\sigma + U)\Gamma_{L\sigma} + f_R(E_\sigma + U)\Gamma_{R\sigma}, \\
\tilde{\beta}_{1\sigma} &= (1 - f_L(E_\sigma + U))\Gamma_{L\sigma} + (1 - f_R(E_\sigma))\Gamma_{R\sigma}, \\
\alpha_{2\sigma} &= f_L(E_\sigma)\Gamma_{L\sigma}e^{-i\Phi/2} + f_R(E_\sigma)\Gamma_{R\sigma}e^{i\Phi/2}, \\
\beta_{2\sigma} &= (1 - f_L(E_\sigma))\Gamma_{L\sigma}e^{-i\Phi/2} + (1 - f_R(E_\sigma))\Gamma_{R\sigma}e^{i\Phi/2}, \\
\tilde{\alpha}_{2\sigma} &= f_L(E_\sigma + U)\Gamma_{L\sigma}e^{-i\Phi/2} + f_R(E_\sigma + U)\Gamma_{R\sigma}e^{i\Phi/2}, \\
\tilde{\beta}_{2\sigma} &= (1 - f_L(E_\sigma + U))\Gamma_{L\sigma}e^{-i\Phi/2} \\
&\quad + (1 - f_R(E_\sigma + U))\Gamma_{R\sigma}e^{i\Phi/2}.
\end{aligned} \tag{7}$$

The equations for the tunneling coefficients clearly demonstrate the influence of the magnetic flux Φ in the terms $\alpha_{2,\sigma}$, $\tilde{\alpha}_{2,\sigma}$, $\beta_{2,\sigma}$, and $\tilde{\beta}_{2,\sigma}$ as the relative phase factor $\exp(-i\Phi)$ between the probability amplitude for tunneling into the left and that for tunneling into the right leads.

To numerically calculate the shot noise we first rewrite the quantum rate equations in matrix form:

$$\frac{d\vec{\rho}(t)}{dt} = \mathbf{M}\vec{\rho}(t), \tag{8}$$

where $\vec{\rho}(t)$ is the column vector of the density matrix elements, $\rho_{\sigma\sigma',\sigma''\sigma'''} = \langle\sigma,\sigma'|\hat{\rho}|\sigma'',\sigma'''\rangle$ given in Appendix A. The noise power spectrum for the current is given by Fourier transform of the current-current correlation function:

$$S_{I_{j,a}I_{j',a}}(\omega) = 2\int_{-\infty}^{\infty} dt e^{i\omega t}[\langle I_{j,a}(t)I_{j',a}(0)\rangle - \langle I_{j,a}\rangle\langle I_{j',a}\rangle], \tag{9}$$

where $I_{j,a}$ is either spin or charge current ($a = C,S$) through the lead $j = L,R$. The spin current is defined as

$$I_{j,S} = \frac{\hbar}{2}(I_{j,\uparrow} - I_{j,\downarrow}) = \frac{\hbar}{2}Tr[(\hat{\Gamma}_{j,\uparrow} - \hat{\Gamma}_{j,\downarrow})\vec{\rho}^{(0)}], \tag{10}$$

while the charge current is given by

$$I_{j,C} = e(I_{j,\uparrow} + I_{j,\downarrow}) = eTr[(\hat{\Gamma}_{j,\uparrow} + \hat{\Gamma}_{j,\downarrow})\vec{\rho}^{(0)}], \tag{11}$$

where $\vec{\rho}^{(0)}$ is the steady-state solution of Eq. (8) given by the eigenvector of the 0 eigenvalue of $\mathbf{M}$. The current operator $\hat{\Gamma}_{j,\sigma}$ contains the rates for spin σ electron tunneling across the $j = L,R$ lead into or out of the appropriate states of the dots. These operators are completely defined by the rate of change of the populations due to tunneling, with detailed expressions given in Appendix A.

By introduction of the time evolution operator $\hat{T}(t) = \exp[\mathbf{M}t]$ and subsequent spectral decomposition of matrix $\mathbf{M}$, one obtains the expression for the shot noise spectrum,[24]

$$\begin{aligned}
S_{I_{j,\sigma}I_{j',\sigma'}}(\omega) &= \delta_{j,j'}\delta_{\sigma,\sigma'}2sI_{j,\sigma} + 2s^2\sum_{\lambda\neq0}\left(\frac{Tr[\hat{\Gamma}_{j,\sigma}\hat{P}_\lambda\hat{\Gamma}_{j',\sigma'}\vec{\rho}^{(0)}]}{-i\omega - \lambda}\right. \\
&\quad \left. + \frac{Tr[\hat{\Gamma}_{j',\sigma'}\hat{P}_\lambda\hat{\Gamma}_{j,\sigma}\vec{\rho}^{(0)}]}{i\omega - \lambda}\right),
\end{aligned} \tag{12}$$

where $s = e$ for the charge current and $s = \frac{\hbar}{2}$ for the spin current. Here the λ's are the eigenvalues of matrix $\mathbf{M}$, while $\hat{P}_\lambda$ is the projection matrix that projects a vector onto the subspace spanned by the eigenvalue λ.

The Fano factor, which measures the ratio of the actual shot noise to the Poissonian Schottky noise of uncorrelated particles, $2sI$, is given by

$$F_{C(S)}(\omega) = \frac{S_{C(S)}(\omega)}{2sI_{C(S)}}, \tag{13}$$

where $S_{C(S)}(\omega)$ is the charge (C) or spin (S) shot noise in the right lead. Because the number of electrons passing from the left to the right lead is conserved, both the average current and the shot noise are identical in both leads.

III. RESULTS

In Sec. III A we examine the current vs. lead voltage and shot noise for the particular case of zero magnetic flux in detail, and then in Sec. III B we examine how nonzero AB flux modifies these results. In all our calculations, we set the tunneling rates between the leads and the dots to be equal, $\Gamma_{L(R)\sigma} = \Gamma$, and use Γ as the energy/time scale relative to which all energies and frequencies are measured. We therefore calculate the charge current I_C in units of $e\Gamma$ and the spin current I_S in units of $\hbar\Gamma/2$. We consider the dots to be identical, with the single-electron level $E_d = 5$, Zeeman splitting $\Omega = 4$, and interdot Coulomb repulsion $U = 20$ (in units of $\hbar\Gamma$). The voltage bias $\Delta V = \mu_L - \mu_R$ across the leads is symmetric about 0 with $\mu_L = -\mu_R$ and is expressed everywhere in units of $\hbar\Gamma/|e|$. Additionally, we consider both unpolarized leads containing both spin polarizations and ferromagnetic leads with identical polarizations or opposite polarizations. Although we have examined both charge and spin shot noise, in the rest of the paper we present only charge shot noise graphs, because the spin shot noise shows the same features as charge noise and does not provide any additional information.

A. Zero flux

In Fig. 3 we show the behavior of spin and charge currents through the device versus ΔV in the absence of the external magnetic flux ($\Phi = 0$) as well as Rabi oscillations ($R_1 = R_2 = 0$) and exchange coupling ($J_n = J_z = 0$) for unpolarized leads. The charge *I-V* curve exhibits an expected "staircase" behavior, ascending in steps and reaching higher and higher plateaus as the potential of the left lead μ_L crosses higher energy levels and opens additional transport channels. Unlike the charge current, the spin current displays a qualitatively different *I-V* curve. For low bias, $\Delta V < 2$, electrons in the leads do not have enough energy to tunnel into the dots, and both spin and charge currents are 0. As the potential of the left lead increases over the single spin-down tunneling energy $E_{\mathrm{TUN}\downarrow} = E_D - \Omega$, only a spin-down electron can enter the dots and the spin current becomes negative, while the charge current is positive. When the left lead potential crosses the value of the spin-up electron tunneling energy $E_{\mathrm{TUN}\uparrow} = E_D + \Omega$, both spin-up and spin-down currents are equal, leading to 0 total spin current but another jump in the charge current. Once μ_L crosses the tunneling energy needed for an additional spin-down electron to tunnel into the single empty dot, $E'_{\mathrm{TUN}\downarrow} = E_\downarrow + U$, three new transport channels open up—$E_{\downarrow\downarrow}$, $E_{\uparrow\downarrow}$, and $E_{\downarrow\uparrow}$—leading to another jump in the charge current. Since only doubly occupied states with at least one spin-down electron are now accessible from the left lead, an "imbalance" between spin-up and spin-down current is established once again and there is a nonzero total spin current. Finally, after a further increase in μ_L of $2\bar{\Omega}$, a second spin-up electron is now able to enter, thereby again restoring the symmetry between spin-up and spin-down electrons. As a result, the spin current again returns to 0 but there is a final jump in the charge current. Figure 4 shows the charge and spin current shot noise in each of the plateau regions, showing sub-Poissonian statistics at zero frequency and Poissonian statistics at finite frequencies.

It is clear from Eq. (1) that the exchange coupling functions only when both dots are occupied by an electron. Therefore to study its effect we let $\Delta V \to \infty$ so that all singly and doubly occupied states are accessible transport channels regardless of the Rabi frequencies and exchange coupling energies. In this case there are no visible effects of the exchange coupling on the total spin and charge currents since no new transport channels are created by either the Rabi spin flips or the exchange coupling. These interactions couple the bare energy eigenstates of the dots, leading to a new basis of energy eigenstates of the same dimension. The same is true of the zero-frequency shot noise. From Fig. 4 one can see that $F(0) \approx 0.77$. The same value of $F(0)$ is obtained for the parameters plotted in Figs. 5, 6, 7, and 8, showing that $F(0)$ is independent of Φ, $R_{1,2}$, J_n, and J_z. $F(0)$ is a direct measure of the number of open transport channels N,

$$F(0) = \frac{\sum_{n=1}^{N} T_n(1 - T_n)}{\sum_{n=1}^{N} T_n}, \tag{14}$$

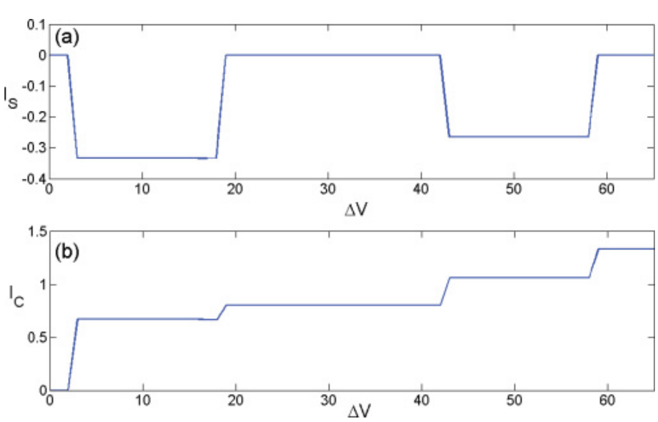

FIG. 3. (Color online) *I-V* curve in the absence of magnetic flux for $U = 20$, $R_1 = R_2 = 0$, and $J_z = J_n = 0$ (unpolarized leads): (a) spin current; (b) charge current. Note that here and in all subsequent figures, I_C is in units of $e\Gamma$ and I_S is in units of $\hbar\Gamma/2$, while ΔV is in units of $\hbar\Gamma/|e|$.

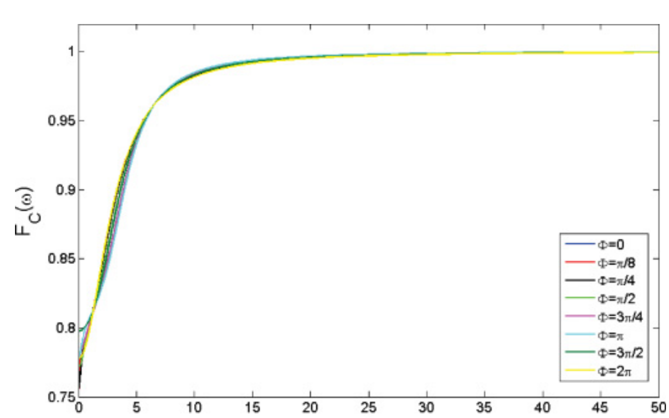

FIG. 4. (Color online) Charge current shot noise as a function of frequency for $U = 20$, $R_1 = R_2 = 0$, $J_z = J_n = 0$, and different values of magnetic flux (unpolarized leads). Note that here and in all subsequent figures, ω is measured in units of Γ.

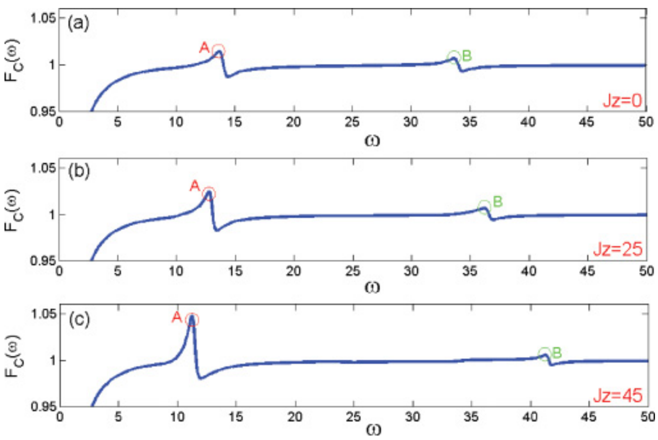

FIG. 5. (Color online) Effect of the longitudinal direct spin coupling strength J_z on a charge current shot noise as a function of frequency (identical lead polarizations): (a) $J_z = 0$, (b) $J_z = 25$, and (c) $J_z = 45$. For all graphs $\Delta V = 80$, $\Phi = 0$, $U = 20$, $R_1 = 7$, $R_2 = 17$, and $J_n = 0$.

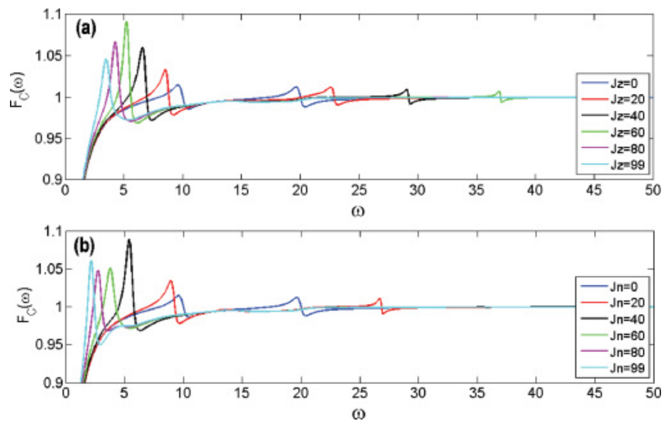

FIG. 7. (Color online) Charge current shot noise as a function of frequency for $\Delta V = 80$, interdot Coulomb blockade $U = 20$, AB phase $\Phi = 0$, and Rabi frequencies $R_1 = 10$ and $R_2 = 5$ (identical lead polarizations): (a) for the range of values of parameter J_z; (b) for the range of values of parameter J_n.

where T_n is the transmission probability through one of the open channels and is not expected to depend on the interactions in the large bias limit.

However, the effects of both intradot spin flips and exchange coupling between dots do manifest themselves in the frequency-dependent shot noise as shown in Figs. 5–8. In the absence of Rabi oscillations the shot noise is sub-Poissonian in the low-frequency range and quickly becomes Poissonian at higher frequencies. In the case of nonzero-spin Rabi flopping and $\Delta V \to \infty$, the shot noise spectrum exhibits structures characteristic of Fano resonances visible at frequencies equal to twice the Rabi frequencies, $\omega = 2R_i$, $i = 1,2$, when the leads are spin polarized (in the case of unpolarized leads, there is no observable effect even for the spin current). Similar finite-frequency shot noise resonances have been studied for spin Rabi flopping in a single QD[30] and for double QDs in series with interdot tunneling[24] and can be explained as follows: For leads with identical spin polarization, an electron can only exit through the right lead, allowing another electron to enter the same dot if it undergoes either no Rabi flopping or a full 2π Rabi oscillation. The case of no Rabi oscillation contributes only to the zero-frequency noise. For leads of opposite polarization, two successive electrons must undergo one-half of a Rabi oscillation to exit leading to current correlations at intervals $\pi/2R_i + \pi/2R_i = \pi/R_i$. The current therefore exhibits positive super-Poissonian correlations at time intervals π/R_i corresponding to a frequency $\omega = 2R_i$.

In the same figures one can also see how exchange coupling affects these resonances. As shown in Fig. 5, an increase in the longitudinal coupling J_z affects the position of the structures in the shot noise, moving them away from each other by shifting the low-frequency structure toward even lower frequencies and the high frequency one toward even higher frequencies. This can be qualitatively understood by noting that the longitudinal coupling shifts the Zeeman splitting of

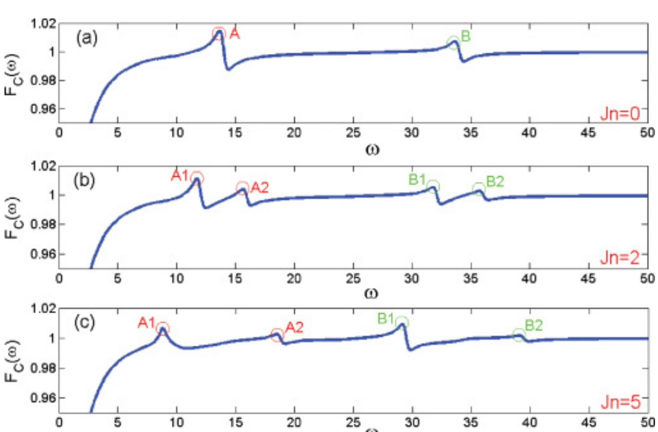

FIG. 6. (Color online) Effect of the transversal direct spin coupling strength J_n on a charge current shot noise as a function of frequency (identical lead polarizations): (a) $J_n = 0$, (b) $J_n = 2$, and (c) $J_n = 5$. For all graphs $\Delta V = 80$, $\Phi = 0$, $U = 20$, $R_1 = 7$, $R_2 = 17$, and $J_z = 0$.

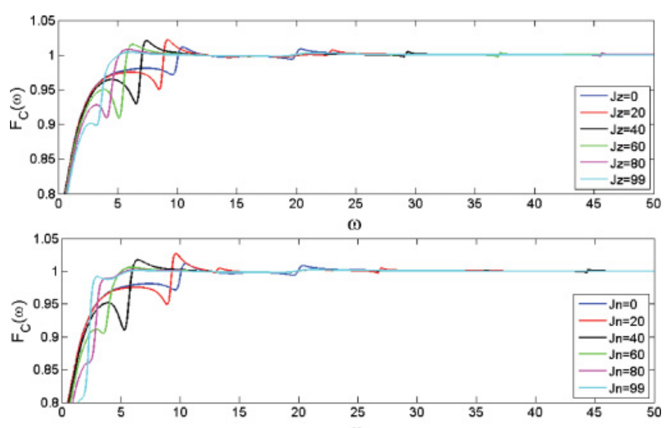

FIG. 8. (Color online) Charge current shot noise as a function of frequency for $\Delta V = 80$, interdot Coulomb blockade $U = 20$, AB phase $\Phi = 0$, and Rabi frequencies $R_1 = 10$ and $R_2 = 5$ (opposite lead polarizations): (a) for the range of values of parameter J_z; (b) for the range of values of parameter J_n.

each spin by an amount $\pm J_z$ depending on the orientation of the spin in the adjacent dot, leading to off-resonant Rabi oscillations at the frequencies $\sqrt{R_i^2 + (\Delta \pm J_z)^2}$. Changing the value of the transverse exchange coupling J_n affects not only the position but also the number of non-Poissonian resonances in the shot noise as shown in Fig. 6. When $R_1 \neq R_2$ there are two Fano-shaped structures in the shot noise spectrum [see Fig. 6(a)], but once J_n becomes nonzero, each of the structures bifurcates into two resonances located symmetrically around $\omega = 2R_i$ separated by $2J_n$. Since the transverse exchange J_n represents nonlinear Rabi oscillations where the spin state of the first dot undergoes oscillations conditioned on the presence of another electron in the second dot, which also Rabi flops in response to the first electron, J_n acts in conjunction with the single-spin linear Rabi flopping to give rise to Rabi oscillations at the frequencies $R_i \pm J_n$, where the $\pm$ results from the relative orientations of the spins.

Finally, it is worth remarking on the effect the polarization of the leads has on the shape of the resonances. In Fig. 7(a) we have plotted the shot noise for a range of J_z in the case of identical polarization, and in Fig. 8(a), for the case of opposite polarization. Figures 7(b) and 8(b) also show the shot noise for the same polarizations but for a range of J_n. In both cases one can see that the shapes of the resonances are inverted when leads are changed from identical polarization to opposite polarization; that is, for identical polarization the peak feature of the structure is followed by the dip feature, while in the case of opposite polarization the dip precedes the peak. This is not unique to the case of zero magnetic flux either, as one can see from Figs. 12(a) and 12(b) in the next section, where the shape of the resonances are inverted when the lead polarizations are changed, irrespective of the flux through the interferometer. For identical lead polarizations the dominant super-Poissonian peaks representing bunching of electrons change to a sub-Poissonian antibunching when the polarization of the right lead is inverted. For identical polarizations it is easy for successive electrons to transit through the dot since a spin flip is not necessary, leading to bunching, whereas for opposite polarizations a spin flip becomes necessary for each of the electrons, leading to an increase in the time between electron arrivals and hence antibunching of the arrival times in the lead.

B. Finite flux

The spin and charge *I-V* curves for different values of Φ are shown in Figs. 9 and 10. Here we draw attention to two distinct cases: one when there is a difference between the Rabi frequencies (Fig. 9) and the other where the Rabi frequencies are identical (Fig. 10). In the former case, shown in Fig. 9, the *I-V* curve is completely independent of Φ, indicative of no interference between paths in the conductance. The absence of flux-dependent interference is because the difference in the Rabi frequencies introduces clear "which-way" information for the path an electron takes in the form of the spin orientation of the electron exiting the interferometer. For identical Rabi frequencies (Fig. 10) there is no distinction between the two dots, and which-way information is not present. In this case one can see the strong dependence of the charge current on the AB flux. The spin current exhibits interference only in the

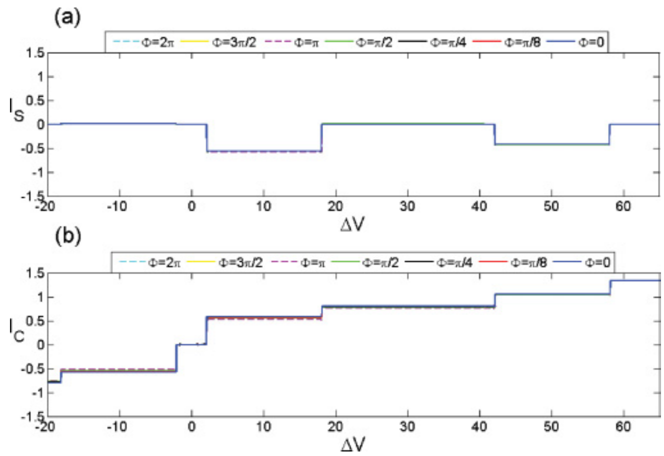

FIG. 9. (Color online) *I-V* curve for $U = 20$, $R_1 = 10$, $R_2 = 5$, $J_n = J_z = 0$, and different values of AB flux (unpolarized leads): (a) spin current; (b) charge current.

bias ranges where there is an unbalanced number of transport channels for spin-down electrons.

Figures 11(a)–11(c) show I_C as a function of (Φ) for three different ΔV values for $J_n = J_z = 0$ and $R_1 = R_2 = 0$. In Fig. 11(a), where $E_d - \Omega < \Delta V < E_d + U - \Omega$, there is only single-electron occupancy of the interferometer, resulting in a high-contrast interference pattern with constructive interference at integer multiples of 2π and total destructive interference at odd multiples of π. In the transitional regime, $E_d + U - \Omega < \Delta V < E_d + U + \Omega$, where all doubly occupied states except $|\uparrow_1, \uparrow_2\rangle$ ae allowed, an AB interference pattern is still visible, but now total destructive interference occurs only at integer multiples of 4π. For large bias values, $\Delta V > E_d + U + \Omega$, all doubly occupied states are equally probable and there are no AB oscillations, since the Coulomb blockade causes the two electrons to be partitioned equally between the dots with zero probability of two electrons on the same dot. In this context the partial interference shown in Fig. 11(b) can be attributed to the absence of $|\uparrow_1, \uparrow_2\rangle$. Equal nonzero Rabi oscillations do not change I_C vs. Φ, while an increase in the difference between the two Rabi frequencies

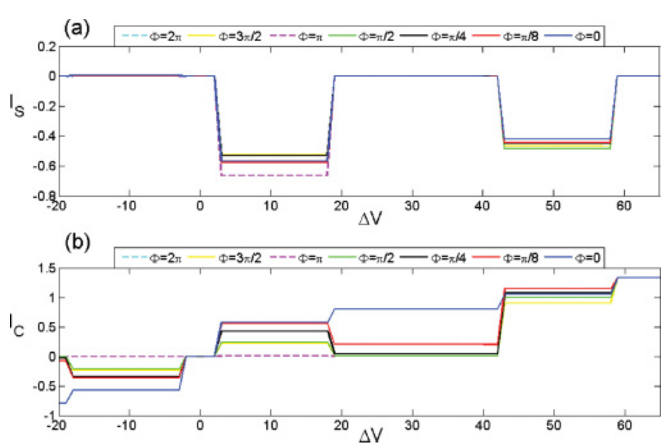

FIG. 10. (Color online) *I-V* curve for $U = 20$, $R_1 = 10$, $R_2 = 10$, $J_n = J_z = 0$, and different values of AB flux (unpolarized leads): (a) spin current; (b) charge current.

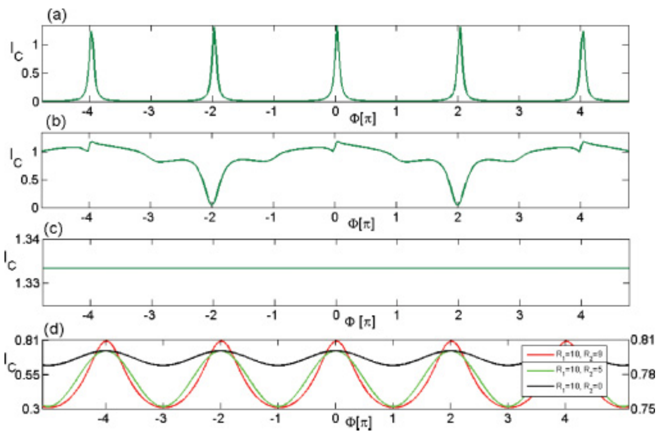

FIG. 11. (Color online) Charge current as a function of AB flux (in units of π) for $U = 20$, $R_1 = R_2 = 0$, $J_n = 0$, and $J_z = 0$ (unpolarized leads): (a) small bias, $\Delta V = 20$; (b) medium bias, $\Delta V = 46$; (c) large bias, $\Delta V = 80$; and (d) small bias, $\Delta V = 20$, with different Rabi frequencies ($R_1 = R_2 = 10$ on the left, y axis; $R_1 = 10$, $R_2 = 5$ and $R_1 = 10$, $R_2 = 0$ on the right axis).

makes the AB oscillation more harmonic while reducing the amplitude of the oscillations since, again, the difference between R_1 and R_2 provides which-way information for the interferometer. This is shown in Fig. 11(d).

The effect of Φ on the shot noise in the limit of very large bias ($\Delta V \to \infty$) is shown in Fig. 12. While $F(0)$ is unaffected by the AB flux, there is a reduction in the size of the Fano-style resonances at finite frequency. In the case of identical lead polarizations [Fig. 12(a)], as the flux increases to $\Phi = \pi$ there is a dramatic attenuation of the amplitude of the high-frequency resonance, eventually causing the shape of the resonance to invert itself at $\Phi = \pi$. The low-frequency resonance shows significantly less attenuation with increasing Φ. After Φ crosses the value of π the attenuation reverses and the features grow in amplitude again for increasing Φ, returning to their maximum amplitude at $\Phi = 2\pi$. For opposite lead polarizations we have a similar attenuation of the noise resonances, only in this case it is more visible in the lower-frequency structure.

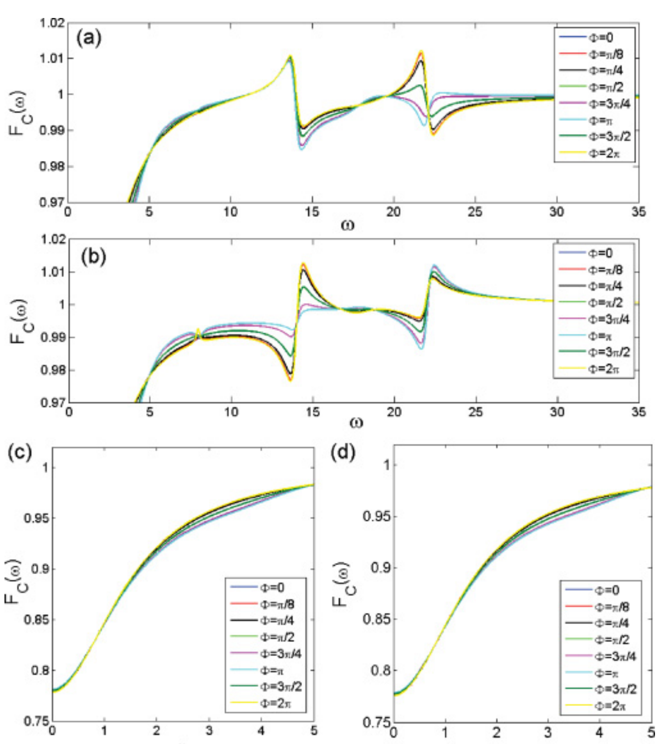

FIG. 12. (Color online) Charge current shot noise as a function of frequency for $\Delta V = 80$, $U = 20$, $R_1 = 7$, $R_2 = 11$, $J_n = 0$, $J_z = 0$, and different values of AB flux: (a) identical lead polarizations and (b) opposite lead polarizations. (c, d) Closeups of (a) and (b), respectively, showing the shot noise for low frequencies.

IV. CONCLUSIONS

We have examined a ballistic electron double-dot AB interferometer with a focus on the effect that interdot spin-spin interactions and intradot spin flips have on the current- and frequency-dependent current shot noise. Direct spin exchange coupling (J_z and J_n) have no effect on either the spin or charge currents or the zero-frequency shot noise but do affect the shot noise at finite frequencies. For nonzero intradot spin flips, the shot noise displays characteristic resonances at twice the Rabi frequencies whose positions are shifted by J_z and are split into pairs of resonances by J_n. These results indicate that spin interactions between QDs can be measured directly from the finite-frequency charge shot noise. The effect of finite AB flux through the interferometer also affects the shot noise resonances, leading to an attenuation of their amplitude for phases increasing from 0 to π, reflecting increased destructive interference, while the amplitudes again grow in the interval π to 2π as destructive interference gives way to constructive interference.

Experiments have already been performed on parallel coupled QDs that function as an AB interferometer[4,5,7] and on double dots with spin exchange interaction due to tunneling of electrons between the dots,[26] both using gate-defined QDs in two-dimensional electron gases formed at AlGaAs/GaAs interfaces. In fact, the AB interferometer experiments[4,5,7] also included a tunable tunnel coupling between dots but the experiments did not study the spin state, whereas the latter experiment[26] explicitly used the tunnel coupling to lift the degeneracy between spin singlet and spin triplet states to coherently control the two-electron spin states of the double dot. What would be required for our model is to repeat the previous experiments,[4,5,7] but with spin polarized leads. In the last decade there have been numerous demonstrations of spin injection and spin measurements in semiconductors.[31] Injection of spin-polarized charge carriers into nonmagnetic GaAs leads can be achieved either from a ferromagnetic doped semiconductor layer such as GaMnAs[32] or from ferromagnetic metallic layers such as CoFe via a tunnel barrier.[33]

In a future work we will quantify the level entanglement between the dots and how the shot noise spectrum correlates with the measures of entanglement. It has been shown[34] that the entanglement of two electrons in the double dot can be detected in noise measurements, where singlet and triplet states lead to noise contributions of opposite signs. By appropriate control of the AB phase, interdot Coulomb repulsion, and interdot spin-spin coupling, one can manipulate the probability amplitudes for the different tunneling paths of the interferometer and the probability of formation of interdot entangled spin triplet and singlet states.

ACKNOWLEDGMENTS

The authors would like to thank Professor Ting Yu for very useful discussions. We also wish to extend our gratitude to Mike Gargano and Patrick Hawkins for all the help they provided in producing some of the graphs. This work was supported by National Science Foundation Award No. 0757933.

APPENDIX A: CURRENT OPERATORS

Current operators $\hat{\Gamma}_{L(R)\sigma}$ are given by 33×33 sparse matrices with all of the elements $\Gamma_{L(R)\sigma}(i,j)$ equal to 0 except the following.

The left spin-up current operator $\hat{\Gamma}_{L\uparrow}$:

$$\Gamma_{L\uparrow}(1,2) = -(1 - f_L(E_\uparrow))\Gamma_{L\uparrow},$$
$$\Gamma_{L\uparrow}(1,4) = -(1 - f_L(E_\uparrow))\Gamma_{L\uparrow},$$
$$\Gamma_{L\uparrow}(1,6) = -(1 - f_L(E_\uparrow))\Gamma_{L\uparrow}e^{(-i\Phi/2)},$$
$$\Gamma_{L\uparrow}(1,8) = -(1 - f_L(E_\uparrow))\Gamma_{L\uparrow}e^{(+i\Phi/2)},$$
$$\Gamma_{L\uparrow}(2,1) = f_L(E_\uparrow)\Gamma_{L\uparrow},$$
$$\Gamma_{L\uparrow}(2,10) = -(1 - f_L(E_\uparrow + U))\Gamma_{L\uparrow},$$
$$\Gamma_{L\uparrow}(3,13) = -(1 - f_L(E_\uparrow + U))\Gamma_{L\uparrow},$$
$$\Gamma_{L\uparrow}(4,1) = f_L(E_\uparrow)\Gamma_{L\uparrow},$$
$$\Gamma_{L\uparrow}(4,10) = -(1 - f_L(E_\uparrow + U))\Gamma_{L\uparrow},$$
$$\Gamma_{L\uparrow}(5,12) = -(1 - f_L(E_\uparrow + U))\Gamma_{L\uparrow},$$
$$\Gamma_{L\uparrow}(10,2) = f_L(E_\uparrow + U)\Gamma_{L\uparrow},$$
$$\Gamma_{L\uparrow}(10,4) = f_L(E_\uparrow + U)\Gamma_{L\uparrow},$$
$$\Gamma_{L\uparrow}(10,6) = f_L(E_\uparrow + U)\Gamma_{L\uparrow}e^{(-i\Phi/2)},$$
$$\Gamma_{L\uparrow}(10,8) = f_L(E_\uparrow + U)\Gamma_{L\uparrow}e^{(i\Phi/2)},$$
$$\Gamma_{L\uparrow}(12,5) = f_L(E_\uparrow + U)\Gamma_{L\uparrow},$$
$$\Gamma_{L\uparrow}(13,3) = f_L(E_\uparrow + U)\Gamma_{L\uparrow}.$$

The left spin-down current operator $\hat{\Gamma}_{L\downarrow}$:

$$\Gamma_{L\downarrow}(1,3) = -(1 - f_L(E_\downarrow))\Gamma_{L\downarrow},$$
$$\Gamma_{L\downarrow}(1,5) = -(1 - f_L(E_\downarrow))\Gamma_{L\downarrow},$$
$$\Gamma_{L\downarrow}(1,7) = -(1 - f_L(E_\downarrow))\Gamma_{L\downarrow}e^{(-i\Phi/2)},$$
$$\Gamma_{L\downarrow}(1,9) = -(1 - f_L(E_\downarrow))\Gamma_{L\downarrow}e^{(+i\Phi/2)},$$
$$\Gamma_{L\downarrow}(2,12) = -(1 - f_L(E_\downarrow + U))\Gamma_{L\downarrow},$$
$$\Gamma_{L\downarrow}(3,1) = f_L(E_\downarrow)\Gamma_{L\downarrow},$$
$$\Gamma_{L\downarrow}(3,11) = -(1 - f_L(E_\downarrow + U))\Gamma_{L\downarrow},$$
$$\Gamma_{L\downarrow}(4,13) = -(1 - f_L(E_\downarrow + U))\Gamma_{L\downarrow},$$
$$\Gamma_{L\downarrow}(5,1) = f_L(E_\downarrow)\Gamma_{L\downarrow},$$
$$\Gamma_{L\downarrow}(5,11) = -(1 - f_L(E_\downarrow + U))\Gamma_{L\downarrow},$$
$$\Gamma_{L\downarrow}(11,3) = f_L(E_\downarrow + U)\Gamma_{L\downarrow},$$
$$\Gamma_{L\downarrow}(11,5) = f_L(E_\downarrow + U)\Gamma_{L\downarrow},$$
$$\Gamma_{L\downarrow}(11,7) = f_L(E_\downarrow + U)\Gamma_{L\downarrow}e^{(-i\Phi/2)},$$
$$\Gamma_{L\downarrow}(11,9) = f_L(E_\downarrow + U)\Gamma_{L\downarrow}e^{(i\Phi/2)},$$
$$\Gamma_{L\downarrow}(12,2) = f_L(E_\downarrow + U)\Gamma_{L\downarrow},$$
$$\Gamma_{L\downarrow}(13,4) = f_L(E_\downarrow + U)\Gamma_{L\downarrow}.$$

The right spin-up current operator $\hat{\Gamma}_{R\uparrow}$:

$$\Gamma_{R\uparrow}(1,2) = (1 - f_R(E_\uparrow))\Gamma_{R\uparrow},$$
$$\Gamma_{R\uparrow}(1,4) = (1 - f_R(E_\uparrow))\Gamma_{R\uparrow},$$
$$\Gamma_{R\uparrow}(1,6) = (1 - f_R(E_\uparrow))\Gamma_{R\uparrow}e^{(+i\Phi/2)},$$
$$\Gamma_{R\uparrow}(1,8) = (1 - f_R(E_\uparrow))\Gamma_{R\uparrow}e^{(-i\Phi/2)},$$
$$\Gamma_{R\uparrow}(2,1) = -f_R(E_\uparrow)\Gamma_{R\uparrow},$$
$$\Gamma_{R\uparrow}(2,10) = (1 - f_R(E_\uparrow + U))\Gamma_{R\uparrow},$$
$$\Gamma_{R\uparrow}(3,13) = (1 - f_R(E_\uparrow + U))\Gamma_{R\uparrow},$$
$$\Gamma_{R\uparrow}(4,1) = -f_R(E_\uparrow)\Gamma_{R\uparrow},$$
$$\Gamma_{R\uparrow}(4,10) = (1 - f_R(E_\uparrow + U))\Gamma_{R\uparrow},$$
$$\Gamma_{R\uparrow}(5,12) = (1 - f_R(E_\uparrow + U))\Gamma_{R\uparrow},$$
$$\Gamma_{R\uparrow}(10,2) = -f_R(E_\uparrow + U)\Gamma_{R\uparrow},$$
$$\Gamma_{R\uparrow}(10,4) = -f_R(E_\uparrow + U)\Gamma_{R\uparrow},$$
$$\Gamma_{R\uparrow}(10,6) = -f_R(E_\uparrow + U)\Gamma_{R\uparrow}e^{(+i\Phi/2)},$$
$$\Gamma_{R\uparrow}(10,8) = -f_R(E_\uparrow + U)\Gamma_{R\uparrow}e^{(-i\Phi/2)},$$
$$\Gamma_{R\uparrow}(12,5) = -f_R(E_\uparrow + U)\Gamma_{R\uparrow},$$
$$\Gamma_{R\uparrow}(13,3) = -f_R(E_\uparrow + U)\Gamma_{R\uparrow}.$$

The right spin-down current operator $\hat{\Gamma}_{R\downarrow}$:

$$\Gamma_{R\downarrow}(1,3) = (1 - f_R(E_\downarrow))\Gamma_{R\downarrow},$$
$$\Gamma_{R\downarrow}(1,5) = (1 - f_R(E_\downarrow))\Gamma_{R\downarrow},$$
$$\Gamma_{R\downarrow}(1,7) = (1 - f_R(E_\downarrow))\Gamma_{R\downarrow}e^{(+i\Phi/2)},$$
$$\Gamma_{R\downarrow}(1,9) = (1 - f_R(E_\downarrow))\Gamma_{R\downarrow}e^{(-i\Phi/2)},$$
$$\Gamma_{R\downarrow}(2,12) = (1 - f_R(E_\downarrow + U))\Gamma_{R\downarrow},$$
$$\Gamma_{R\downarrow}(3,1) = -f_R(E_\downarrow)\Gamma_{R\downarrow},$$
$$\Gamma_{R\downarrow}(3,11) = (1 - f_R(E_\downarrow + U))\Gamma_{R\downarrow},$$
$$\Gamma_{R\downarrow}(4,13) = (1 - f_R(E_\downarrow + U))\Gamma_{R\downarrow},$$
$$\Gamma_{R\downarrow}(5,1) = -f_R(E_\downarrow)\Gamma_{R\downarrow},$$
$$\Gamma_{R\downarrow}(5,11) = (1 - f_R(E_\downarrow + U))\Gamma_{R\downarrow},$$
$$\Gamma_{R\downarrow}(11,3) = -f_R(E_\downarrow + U)\Gamma_{R\downarrow},$$
$$\Gamma_{R\downarrow}(11,5) = -f_R(E_\downarrow + U)\Gamma_{R\downarrow},$$
$$\Gamma_{R\downarrow}(11,7) = -f_R(E_\downarrow + U)\Gamma_{R\downarrow}e^{(+i\Phi/2)},$$
$$\Gamma_{R\downarrow}(11,9) = -f_R(E_\downarrow + U)\Gamma_{R\downarrow}e^{(-i\Phi/2)},$$
$$\Gamma_{R\downarrow}(12,2) = -f_R(E_\downarrow + U)\Gamma_{R\downarrow},$$
$$\Gamma_{R\downarrow}(13,4) = -f_R(E_\downarrow + U)\Gamma_{R\downarrow}.$$

The density matrix in vector form, which defines the basis for the current operators, is given by $\vec{\rho}^T = [\rho_{0000}, \rho_{\uparrow 0,\uparrow 0}, \rho_{\downarrow 0,\downarrow 0}, \rho_{0\uparrow,0\uparrow}, \rho_{0\downarrow,0\downarrow}, \rho_{\uparrow 0,0\uparrow}, \rho_{\downarrow 0,0\downarrow}, \rho_{0\uparrow,\uparrow 0}, \rho_{0\downarrow,\downarrow 0}, \rho_{\uparrow\uparrow,\uparrow\uparrow}, \rho_{\downarrow\downarrow,\downarrow\downarrow},$

$\rho_{\uparrow\downarrow,\uparrow\downarrow},\rho_{\downarrow\uparrow,\downarrow\uparrow},\rho_{\uparrow\downarrow,\downarrow\uparrow},\rho_{\downarrow\uparrow,\uparrow\downarrow},\rho_{\uparrow 0,\downarrow 0},\rho_{0\uparrow,0\downarrow},\rho_{0\uparrow,\downarrow 0},\rho_{0\downarrow,\uparrow 0},$
$\rho_{\downarrow 0,\uparrow 0},\rho_{0\downarrow,0\uparrow},\rho_{\downarrow 0,0\uparrow},\rho_{\uparrow 0,0\downarrow},\rho_{\uparrow\uparrow,\uparrow\downarrow},\rho_{\uparrow\downarrow,\uparrow\uparrow},\rho_{\uparrow\uparrow,\downarrow\uparrow},\rho_{\downarrow\uparrow,\uparrow\uparrow},$
$\rho_{\uparrow\uparrow,\downarrow\downarrow},\rho_{\downarrow\downarrow,\uparrow\uparrow},\rho_{\uparrow\downarrow,\downarrow\downarrow},\rho_{\downarrow\downarrow,\uparrow\downarrow},\rho_{\downarrow\uparrow,\downarrow\downarrow},\rho_{\downarrow\downarrow,\downarrow\uparrow}]$.

APPENDIX B: MATRIX M

Matrix M is a 33×33 sparse matrix with the following nonzero elements $M(i,j)$:

$$M(2,1) = M(4,1) = \alpha_{1\uparrow}, \quad M(3,1) = M(5,1) = \alpha_{1\downarrow},$$
$$M(1,2) = M(1,4) = \beta_{1\uparrow}, \quad M(1,3) = M(1,5) = \beta_{1\downarrow},$$
$$M(8,1) = M(6,1)^* = \alpha_{2\uparrow}, \quad M(9,1) = M(7,1)^* = \alpha_{2\downarrow},$$
$$M(1,6) = M(1,8)^* = \beta_{2\uparrow}, \quad M(1,7) = M(1,9)^* = \beta 2\downarrow,$$
$$M(10,2) = M(10,4) = M(12,5) = M(13,3) = \tilde{\alpha}_{1\uparrow},$$
$$M(11,3) = M(11,5) = M(12,2) = M(13,4) = \tilde{\alpha}_{1\downarrow},$$

$$\begin{aligned}M(2,10) &= M(3,13) = M(4,10) = M(5,12)\\ &= -\tfrac{1}{2}M(10,10) = \tilde{\beta}_{1\uparrow},\\ M(2,12) &= M(3,11) = M(4,13) = M(5,11)\\ &= -\tfrac{1}{2}M(11,11) = \tilde{\beta}_{1\downarrow},\end{aligned}$$

$$M(10,6) = M(10,8)^* = M(14,9)^* = M(15,7) = \tilde{\alpha}_{2\uparrow},$$
$$M(11,7) = M(11,9)^* = M(14,6) = M(15,8)^* = \tilde{\alpha}_{2\downarrow},$$
$$M(6,10)^* = M(7,14)^* = M(8,10) = M(9,15) = \tilde{\beta}_{2\uparrow},$$
$$M(6,15)^* = M(7,11)^* = M(8,14) = M(9,11) = \tilde{\beta}_{2\downarrow},$$

$$\begin{aligned}M(2,2) &= M(4,4) = M(6,6)^* = M(8,8)\\ &= -(\beta_{1\uparrow} + \tilde{\alpha}_{1\uparrow} + \tilde{\alpha}_{1\downarrow}),\\ M(3,3) &= M(5,5) = M(7,7)^* = M(9,9)\\ &= -(\beta_{1\downarrow} + \tilde{\alpha}_{1\uparrow} + \tilde{\alpha}_{1\downarrow}),\\ M(2,6) &= M(2,8)^* = M(4,6) = M(4,8)^* = M(6,2)^*\\ &= M(6,4)^* = M(8,2) = M(8,4) = -\tfrac{1}{2}(\beta_{2\uparrow} + \tilde{\alpha}_{2\uparrow}),\\ M(3,7) &= M(3,9)^* = M(5,7) = M(5,9)^* = M(7,3)^*\\ &= M(7,5)^* = M(9,3) = M(9,5) = -\tfrac{1}{2}(\beta_{2\downarrow} + \tilde{\alpha}_{2\downarrow}),\end{aligned}$$

$$M(1,1) = -2(\alpha_{1\uparrow} + \alpha_{1\downarrow}),$$
$$M(12,12) = M(13,13) = -(\tilde{\beta}_{1\uparrow} + \tilde{\beta}_{1\downarrow}),$$
$$M(14,14) = M(15,15)^* = -(\tilde{\beta}^*_{2\uparrow} + \tilde{\beta}_{2\downarrow}),$$

$$\begin{aligned}M(16,16) &= M(20,20)^* = M(17,17) = M(21,21)^*\\ &= M(18,18) = M(22,22)^* = M(19,19)^*\\ &= M(23,23) = \tfrac{1}{2}M(28,28) = \tfrac{1}{2}M(29,29)^*\\ &= -2i\Omega,\\ M(24,24) &= M(25,25)^* = M(26,26) = M(27,27)^*\\ &= -i\left(2\Omega + \frac{J_z}{2}\right),\\ M(30,30) &= M(31,31)^* = M(32,32) = M(33,33)^*\\ &= -i\left(2\Omega - \frac{J_z}{2}\right),\end{aligned}$$

$$\begin{aligned}M(12,24) &= -M(12,15) = M(13,15) = -M(13,14)\\ &= M(14,12) = -M(14,13) = M(15,13)\\ &= -M(15,12) = M(24,26) = -M(25,27)\\ &= M(26,24) = -M(27,25) = -M(30,32)\\ &= M(31,33) = -M(32,30) = M(33,31) = iJ_n,\\ M(2,16) &= -M(2,20) = -M(3,16) = M(3,20)\\ &= -M(6,22) = -M(7,23) = M(8,18)\\ &= M(9,19) = M(10,26) = -M(10,27)\\ &= M(11,31) = -M(11,30) = M(12,30)\\ &= -M(12,31) = M(13,27) = -M(13,26)\\ &= M(14,25) = -M(14,33) = M(15,32)\\ &= -M(15,24) = M(16,2) = -M(16,3)\\ &= -M(20,2) = M(20,3) = M(18,8)\\ &= -M(22,6) = M(19,9) = -M(23,7)\\ &= M(24,28) = -M(24,15) = M(25,14)\\ &= -M(25,29) = M(26,10) = -M(26,13)\\ &= M(27,13) = -M(27,10) = M(28,24)\\ &= -M(28,32) = M(29,33) = -M(29,25)\\ &= M(30,12) = -M(30,11) = M(31,11)\\ &= -M(31,12) = M(32,15) - M(32,28)\\ &= M(33,29) = -M(33,14) = iR_1,\\ M(4,17) &= -M(4,21) = -M(5,17)\\ &= M(5,21) = M(6,23) = M(7,22)\\ &= -M(8,19) = -M(9,18) = M(10,24)\\ &= -M(10,25) = M(11,33) = -M(11,32)\\ &= M(12,25) = -M(12,24) = M(13,32)\\ &= -M(13,33) = M(14,30) = -M(14,26)\\ &= M(15,27) = -M(15,31) = M(17,4)\\ &= -M(17,5) = -M(21,4) = M(21,5)\\ &= -M(18,9) = M(22,7) = -M(19,8)\\ &= M(23,6) = M(24,10) = -M(24,12)\\ &= M(25,12) = -M(25,10) = M(26,28)\\ &= -M(26,14) = M(27,15) = -M(27,29)\\ &= M(28,26) = -M(28,30) = M(29,31)\\ &= -M(29,27) = M(30,14) = -M(30,28)\\ &= M(31,29) = -M(31,15) = M(32,13)\\ &= -M(32,11) = M(33,11) = -M(33,13) = iR_2.\end{aligned}$$

*csearch@stevens.edu

[1]C. Beenakker and C. Schonenberger, Phys. Today **56**, 37 (2003); Ya. M. Blanter and M. Buttiker, Phys. Rep. **336**, 1 (2000).
[2]A. Yacoby, M. Heiblum, V. Umansky, H. Shtrikman, and D. Mahalu, Phys. Rev. Lett. **73**, 3149 (1994).
[3]Y. Ji, Y. Chung, D. Sprinzak, M. Heiblum, D. Mahalu, and H. Shtrikman, Nature (London) **422**, 415 (2003).
[4]A. W. Holleitner, R. H. Blick, A. K. Huttel, K. Eber, and J. P. Kotthaus, Science **297**, 70 (2002).
[5]A. W. Holleitner, C. R. Decker, H. Qin, K. Eberl, and R. H. Blick, Phys. Rev. Lett. **87**, 256802 (2001).
[6]J. C. Chen, A. M. Chang, and M. R. Melloch, Phys. Rev. Lett. **92**, 176801 (2004).
[7]R. H. Blick, A. K. Huttel, A. W. Holleitner, E. M. Hohberger, H. Qin, J. Kirschbaum, J. Weber, W. Wegscheider, M. Bichler, K. Eberl, and J. P. Kotthaus, Physica E **16**, 76 (2003).
[8]M. Sigrist, T. Ihn, K. Ensslin, M. Reinwald, and W. Wegscheider, Phys. Rev. Lett. **98**, 036805 (2007).
[9]J. Ma, B. Dong, and X. L. Lei, Eur. Phys. J. B **36**, 599 (2003).
[10]B. Dong, I. Djuric, H. L. Cui, and X. L. Lei, J. Phys. Condens. Matter **16**, 4303 (2004).
[11]B. Dong, X. L. Lei, and N. J. M. Horing, Phys. Rev. B **77**, 085309 (2008).
[12]Y. Tokura, H. Nakano, and T. Kubo, New J. Phys. **9**, 113 (2007).
[13]D. Sztenkiel and R. Swirkowicz, J. Phys. Condens. Matter **19**, 176202 (2007).
[14]H. Lu, R. Lu, and B.-F. Zhu, Phys. Rev. B **71**, 235320 (2005).
[15]J.-L Li and Y.-X. Li, J. Phys. Condens. Matter **20**, 465202 (2008).
[16]B. Kubala and J. Konig, Phys. Rev. B, **65**, 245301 (2002).
[17]D. Urban and J. Konig, Phys. Rev. B **79**, 165319 (2009).
[18]G.-B. Zhang, S.-J. Wang, and L. Li, Phys. Rev. B **74**, 085106 (2006).
[19]B. Dong, X. L. Lei, and N. J. M. Horing, J. Appl. Phys. **104**, 033532 (2008).
[20]L. Qin and Y. Guo, J. Phys. Condens. Matter **20**, 365206 (2008).
[21]F. Bodoky, W. Belzig, and C. Bruder, Phys. Rev. B **77**, 035302 (2008).
[22]B. Dong, H. L. Cui, and X. L. Lei, Phys. Rev. B **69**, 035324 (2004).
[23]P. Meystre and M. Sargent III, *Elements of Quantum Optics*, 3rd ed. (Springer-Verlag, Berlin, 1998).
[24]I. Djuric, B. Dong, and H. L. Cui, J. Appl. Phys. **99**, 063710 (2006).
[25]H. B. Sun and G. J. Milburn, Phys. Rev. B **59**, 10748 (1999).
[26]J. R. Petta, A. C. Johnson, J. M. Taylor, E. A. Laird, A. Yacoby, M. D. Lukin, C. M. Marcus, M. P. Hanson, and A. C. Gossard, Science **309**, 2180 (2005).
[27]G. Burkard and A. Imamoglu, Phys. Rev. B **74**, 041307(R) (2006).
[28]A. Imamoglu, D. D. Awschalom, G. Burkard, D. P. DiVincenzo, D. Loss, M. Sherwin, and A. Small, Phys. Rev. Lett. **83**, 4204 (1999).
[29]O. Gywat, F. Meier, D. Loss, and D. D. Awschalom, Phys. Rev. B **73**, 125336 (2006).
[30]I. Djuric and C. P. Search, Phys. Rev. B **74**, 115327 (2006); I. Djuric, M. Zivkovic, C. P. Search, and G. Recine, *ibid.* **78**, 195316 (2008).
[31]D. D. Awschalom and M. E. Flatte, Nature Phys. **3**, 153 (2007).
[32]Y. Ohno, D. K. Young, B. Beschoten, F. Matsukura, H. Ohno, and D. D. Awschalom, Nature (London) **402**, 790 (1999).
[33]X. Jiang, R. Wang, R. M. Shelby, R. M. Macfarlane, S. R. Bank, J. S. Harris, and S. S. P. Parkin, Phys. Rev. Lett. **94**, 056601 (2005).
[34]D. Loss and E. V. Sukhorukov, Phys. Rev. Lett. **84**, 1035 (2000).